9. A. Boehlen, U. Heinemann, I. Erchova, *J. Neurosci.* **30**, 4585 (2010).
10. J. G. Heys, L. M. Giocomo, M. E. Hasselmo, *J. Neurophysiol.* **104**, 258 (2010).
11. P. D. Dodson, H. Pastoll, M. F. Nolan, *J. Physiol.* **589**, 2993 (2011).
12. T. Hafting, M. Fyhn, T. Bonnevie, M. B. Moser, E. I. Moser, *Nature* **453**, 1248 (2008).
13. A. Jeewajee, C. Barry, J. O'Keefe, N. Burgess, *Hippocampus* **18**, 1175 (2008).
14. H. Stensola *et al.*, *Nature* **492**, 72 (2012).
15. M. P. Brandon *et al.*, *Science* **332**, 595 (2011).
16. J. Koenig, A. N. Linder, J. K. Leutgeb, S. Leutgeb, *Science* **332**, 592 (2011).
17. N. Ulanovsky, C. F. Moss, *Nat. Neurosci.* **10**, 224 (2007).
18. C. Barry, D. Bush, J. O'Keefe, N. Burgess, *Nature* **488**, E1, discussion E2 (2012).
19. E. H. Buhl, J. F. Dann, *Hippocampus* **1**, 131 (1991).
20. C. W. Gatome, L. Slomianka, D. K. Mwangi, H.-P. Lipp, I. Amrein, *Brain Struct. Funct.* **214**, 375 (2010).
21. A. Alonso, R. R. Llinás, *Nature* **342**, 175 (1989).
22. A. Alonso, R. J. Klink, *J. Neurophysiol.* **70**, 128 (1993).
23. C. T. Dickson *et al.*, *J. Neurophysiol.* **83**, 2562 (2000).
24. M. F. Nolan, J. T. Dudman, P. D. Dodson, B. Santoro, *J. Neurosci.* **27**, 12440 (2007).
25. J. S. Haas, A. D. Dorval 2nd, J. A. White, *J. Comput. Neurosci.* **22**, 161 (2007).
26. J. T. Dudman, M. F. Nolan, *PLOS Comput. Biol.* **5**, e1000290 (2009).
27. L. M. Giocomo, M.-B. Moser, E. I. Moser, *Neuron* **71**, 589 (2011).
28. Z. Navratilova, L. M. Giocomo, J. M. Fellous, M. E. Hasselmo, B. L. McNaughton, *Hippocampus* **22**, 772 (2012).
29. C. A. Buckmaster, H. Eichenbaum, D. G. Amaral, W. A. Suzuki, P. R. Rapp, *J. Neurosci.* **24**, 9811 (2004).
30. L. M. Giocomo *et al.*, *Cell* **147**, 1159 (2011).
31. D. L. F. Garden, P. D. Dodson, C. O'Donnell, M. D. White, M. F. Nolan, *Neuron* **60**, 875 (2008).
32. J. C. Magee, *Nat. Neurosci.* **2**, 848 (1999).
33. T. Berger, M. E. Larkum, H. R. Lüscher, *J. Neurophysiol.* **85**, 855 (2001).
34. S. R. Williams, S. R. Christensen, G. J. Stuart, M. Häusser, *J. Physiol.* **539**, 469 (2002).
35. N. A. Otmakhova, J. E. Lisman, *J. Neurophysiol.* **92**, 2027 (2004).
36. W. J. Murphy *et al.*, *Nature* **409**, 614 (2001).
37. L. M. Kay, M. Stopfer, *Semin. Cell Dev. Biol.* **17**, 433 (2006).
38. J. W. Schnupp, C. E. Carr, *Nat. Neurosci.* **12**, 692 (2009).
39. C. Y. Su, K. Menuz, J. R. Carlson, *Cell* **139**, 45 (2009).



**Acknowledgments:** We thank J. Ahn, J. Barcelo, C. Carr, W. Chapman, and M. Roesch for technical assistance and N. Spruston, J.-W. Lin, H. Eichenbaum, C. Stern, T. Gardner, and N. Ulanovsky for advice and comments. N. Ulanovsky and Y. Yovel helped us acquire Egyptian fruit bats for studies in supplementary materials. Research supported by Office of Naval Research grant N00014-12-1-0339 and Multi-disciplinary University Research Initiative N00014-10-1-0936.


**Supplementary Materials**

www.sciencemag.org/cgi/content/full/340/6130/363/DC1
Materials and Methods
Supplementary Text
Figs. S1 to S3
References (*40*–*45*)


10 December 2012; accepted 27 February 2013
10.1126/science.1233831


# Representation of Three-Dimensional Space in the Hippocampus of Flying Bats


**Michael M. Yartsev and Nachum Ulanovsky***



**Many animals, on air, water, or land, navigate in three-dimensional (3D) environments, yet it remains unclear how brain circuits encode the animal's 3D position. We recorded single neurons in freely flying bats, using a wireless neural-telemetry system, and studied how hippocampal place cells encode 3D volumetric space during flight. Individual place cells were active in confined 3D volumes, and in >90% of the neurons, all three axes were encoded with similar resolution. The 3D place fields from different neurons spanned different locations and collectively represented uniformly the available space in the room. Theta rhythmicity was absent in the firing patterns of 3D place cells. These results suggest that the bat hippocampus represents 3D volumetric space by a uniform and nearly isotropic rate code.**


Navigation is crucial for survival, and the need to navigate cuts across the animal kingdom. Several navigational strategies are used by animals, among them maplike navigation (*1*). This strategy relies on a set of brain structures, at the hub of which is the hippocampus (*1*, *2*). This brain area contains "place cells," neurons that activate when the animal enters a restricted region of the environment, the place field (*1*, *2*). Since the discovery of place cells in rodents, these neurons have been reported across mammalian species (*1*–*9*), and their functional properties have been extensively researched (*1*, *2*). However, the spatial and temporal properties of place cells have never been studied in animals moving freely through 3D volumetric space, without any constraints to particular planes of motion. Indeed, in all studies to date, animals have always been navigating on one- or two-dimensional (2D) planes (*1*, *10*)—either horizontal (*5*, *7*, *11*–*15*), tilted (*3*, *4*, *16*–*18*), or vertical (*9*, *13*, *16*)—and thus it remains unresolved how place cells encode the animal's position throughout the entire volume of a 3D volumetric space. We developed wireless recording methodology for freely flying animals (*19*) and recorded single-neuron activity from hippocampal area CA1 of Egyptian fruit bats flying through 3D space.

Bats were tested in one of two setups: either a large cuboid-shaped flight room, where bats performed a naturalistic foraging task (Fig. 1A and fig. S1; room size 580 × 460 × 270 cm; $n$ = 3 bats) or a 3D cubic flight arena of smaller dimensions, where bats searched randomly for food (fig. S2; room size 290 × 280 × 270 cm; $n$ = 2 bats) (*19*). In both setups, bats exhibited complex naturalistic flight trajectories, during which they moved through all the three dimensions of the room (Fig. 1B and fig. S3), traversed large distances (Fig. 1C, left), and flew at high speeds (Fig. 1C, right; and fig. S4). These flight maneuvers resulted in dense and rather uniform coverage of the environment's 3D volume (figs. S5 and S6).

Single-unit activity was recorded from freely flying bats, using a tetrode-based microdrive and a custom lightweight four-channel neural telemetry system designed for flying bats (Fig. 1, D to F, and figs. S7 to S10). The telemetry system allowed the transmission of action potentials from the four channels of one tetrode, with high fidelity (Fig. 1, D, E, and G, and figs. S7 to S9), throughout all the locations in the flight room (figs. S7 and S8) and with very little interference from movement-related noise (fig. S11) (*20*).

The ability to monitor 3D spatial position and record the activity of individual neurons in freely flying bats allowed studying the spatial coding of 3D volumetric space by hippocampal neurons. We recorded a total of 139 well-isolated neurons from five bats in the dorsal CA1 region of the hippocampus (*19*). About half of the cells [73 out of 139 (73/139) or 53%] were active during flight, and 75% of the active cells (55/73) were classified as place cells (fig. S12), becoming active when the bat flew through a restricted volume of the available environment (*19*). Figure 2, A to E, shows the spatial spiking activity of a single hippocampal neuron recorded during flight. This neuron fired nearly exclusively in a confined region of the environment, and this region was restricted in all three dimensions (Fig. 2, A and B, and fig. S13). The firing field of this neuron remained highly stable across the recording session, both in its spatial location and its firing rate (Fig. 2, C and D, and fig. S14A); furthermore, the cell was reliably activated on most of the individual flight passes through the place field (Fig. 2E). Likewise, the majority (75%) of neurons that were active during flight


Department of Neurobiology, Weizmann Institute of Science, Rehovot 76100, Israel.

*Corresponding author. E-mail: nachum.ulanovsky@weizmann.ac.il

exhibited strong spatial tuning (Fig. 2, F to K, and fig. S15), and their firing fields were highly stable throughout the recording session (fig. S14, B and C)—similar to previous reports for rat CA1 place cells (*1*, *22*–*24*).

In both setups, the place fields of different neurons varied in size and location and spanned much of the available 3D space (Fig. 3, A to D). Most place cells discharged within a single 3D firing field (62%; Fig. 3, E and F). The fraction of cells with two or more fields was higher in the large cuboid flight room (43% or 15/35, Fig. 3E) than in the smaller cubic enclosure (30% or 6/20 cells; Fig. 3F; bootstrap test, $P < 0.001$) (*19*), which is in agreement with previous reports in rats, where the number of 2D firing fields increased with the size of the environment (*21*).

Next we asked whether 3D space is represented isotropically in the hippocampus of flying bats; namely, do place fields have the same size in all dimensions? Across the population, the sizes of individual place fields along each of the three cardinal axes of the room were quite similar (Fig. 3, G and H). Utilizing the 3D volumetric coverage of the room by the bats (fig. S1C and fig. S15), we then asked whether 3D place fields are spherical (isotropic), or perhaps anisotropy might be found along some noncardinal axis. We fitted a 3D ellipsoid to the place-field shape, where the ellipsoid was not constrained to be parallel to any of the room walls, and an "elongation index" was defined as the ratio of the longest to the shortest axes of the ellipsoid (fig. S16). To test for the significance of the computed elongation index, we implemented a shuffling procedure in which we randomly redistributed the spikes of the place field along the bat's flight trajectory, constraining them to be within a perfect sphere of the same volume as the ellipsoid, and tested whether the real elongation index was outside the shuffling-based confidence interval (*19*); that is, whether the actual elongation was significantly different from that expected from an underlying perfect sphere, given the animal's behavior (Fig. 3I). Only 9% of the fields (Fig. 3I, red dots; 7/82 fields) showed significant elongation, exhibiting compression along the *z* axis of the room (e.g., neuron 1 in fig. S17C), but sometimes also diagonal field shapes (e.g., neuron 2 in fig. S17C). However, 91% of the place fields in both arenas (75/82 fields) were not significantly different from an underlying sphere (Fig. 3I, green dots; examples in fig. S17C, neurons 3

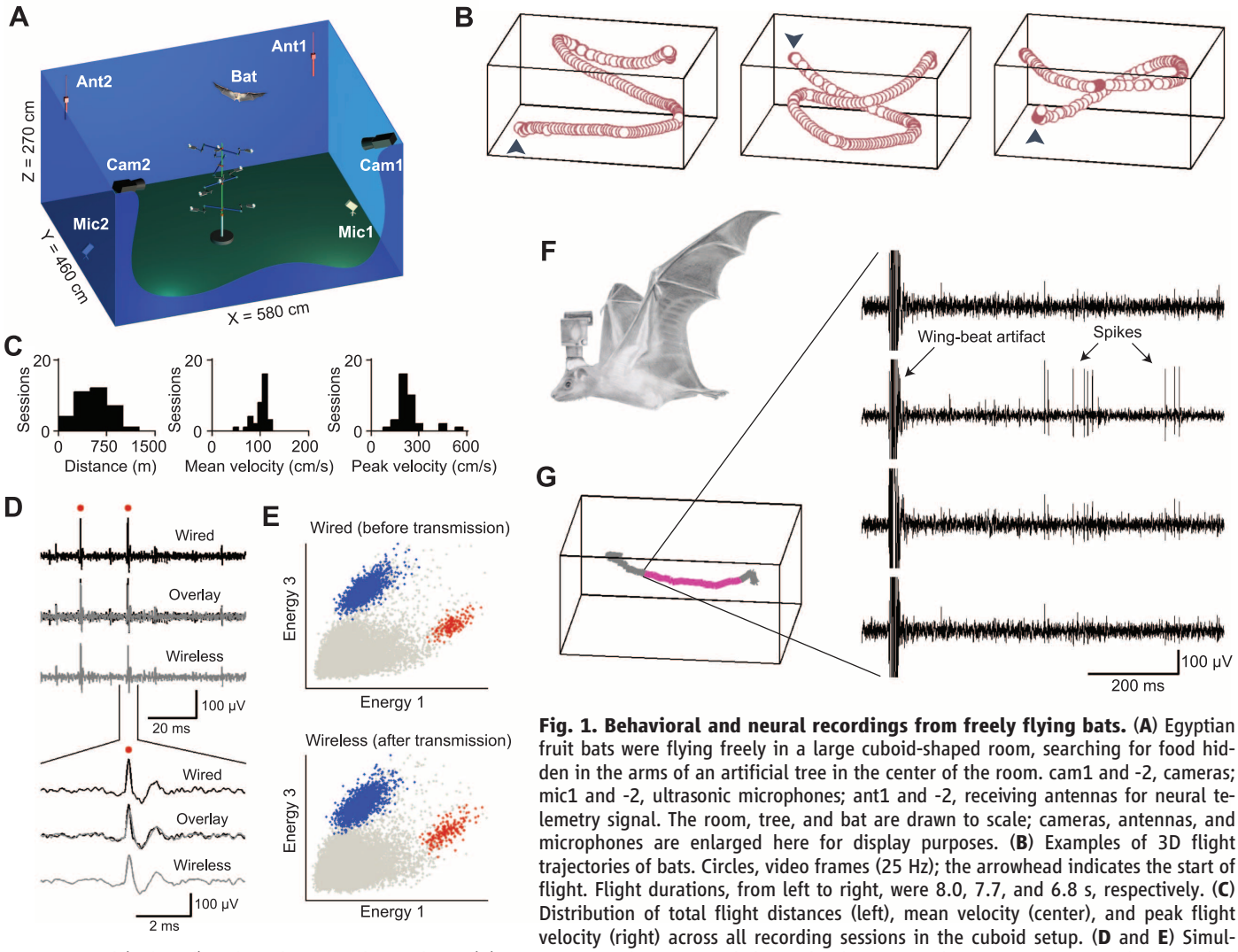


**Fig. 1. Behavioral and neural recordings from freely flying bats.** (**A**) Egyptian fruit bats were flying freely in a large cuboid-shaped room, searching for food hidden in the arms of an artificial tree in the center of the room. cam1 and -2, cameras; mic1 and -2, ultrasonic microphones; ant1 and -2, receiving antennas for neural telemetry signal. The room, tree, and bat are drawn to scale; cameras, antennas, and microphones are enlarged here for display purposes. (**B**) Examples of 3D flight trajectories of bats. Circles, video frames (25 Hz); the arrowhead indicates the start of flight. Flight durations, from left to right, were 8.0, 7.7, and 6.8 s, respectively. (**C**) Distribution of total flight distances (left), mean velocity (center), and peak flight velocity (right) across all recording sessions in the cuboid setup. (**D** and **E**) Simultaneous wired (tethered) and wireless neural recordings. (D) Top: Raw neural trace recorded from bat hippocampal area CA1 from a single channel of the tetrode, before transmission (top), after transmission (bottom), and overlay (center). Bottom: Zoom-in onto a single action potential. (E) 2D projections of spike energies of CA1 neurons, before (top) and after (bottom) wireless transmission. Red and blue dots, clusters corresponding to two neurons; red dots in (E) are spikes from the red cluster. (**F**) Telemetry system on a flying bat, drawn to scale [illustration: S. Kaufman]. (**G**) Neural traces (right) from the four channels of a tetrode, recorded from bat CA1 during one flight segment (left, gray; the magenta portion corresponds to the duration of the neural traces shown on the right).

and 4). Further, comparing the field sizes specifically along the *x*,*y*,*z* cardinal axes of the room showed that, for these 91% of the fields, there was no significant elongation in any of the cardinal directions (fig. S17A; Sign test, $P > 0.15$ for all comparisons). Thus, for the large majority of neurons, 3D place fields were indistinguishable from isotropic spheres.

We next examined whether the locations and sizes of place fields are distributed uniformly across space, as indicated by the population plots in Fig. 3, A to D. Indeed, the size of place fields did not show significant correlation with the distance from the flight-enclosure center, in either of the setups, indicating similar resolution at room center and near the walls (Fig. 3J; correlation coefficient: $r = -0.20$, $P = 0.13$ for the rectangular cuboid flight-room; $r = -0.02$, $P = 0.91$ for the cubic enclosure). Place fields were slightly bigger in the large cuboid flight room than in the smaller cubic flight enclosure (102.3 ± 5.5 cm compared to 94.3 ± 6.9 cm, respectively). Field locations were distributed quite uniformly, both along the radial

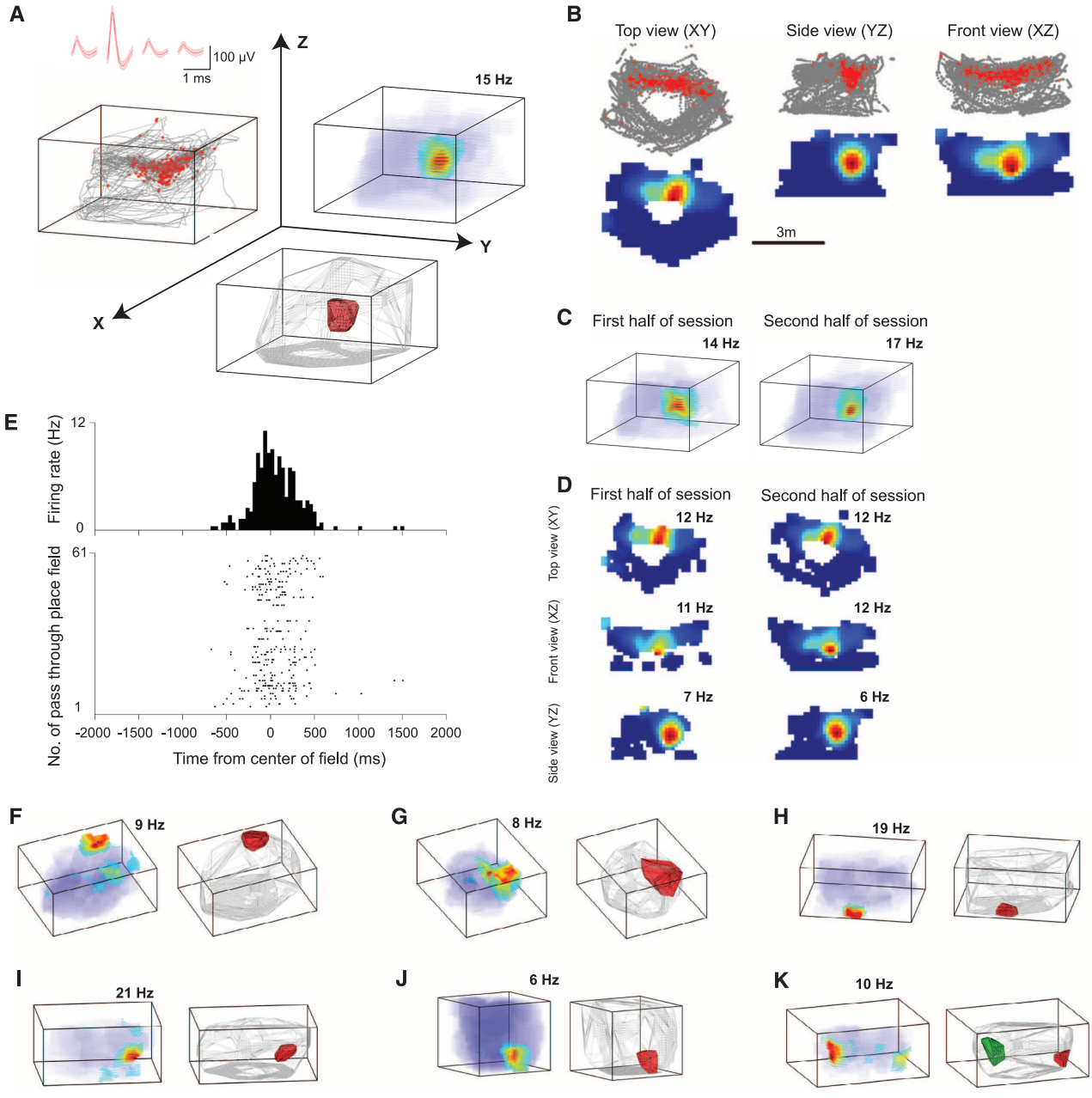


**Fig. 2. Examples of 3D place cells recorded from the hippocampus of flying bats.** (**A** to **E**) An example cell. (A) 3D representation of the neuron's spatial firing. Top left: Spikes (red dots) overlaid on bat's position (gray lines); shown also are the spike waveforms on the four channels of the tetrode (mean ± SD). Top right: 3D color-coded rate map, with peak firing rate indicated. Bottom: Convex hull encompassing the neuron's place field (red polygon) and the volume covered by the bat during flight (gray polygon). (B) 2D projections of the raw data (top) and color-coded rate maps (bottom). (C and D) Stability of the neuron's spatial firing for the first versus second half of the recording session; shown are 3D rate maps (C) and 2D projections (D). Peak firing rate is indicated for each map. (E) Reliability of firing across 61 flight passes through the place field. Bottom: raster plot showing spikes during individual passes (time 0, point closest to field center). Top: Spike density function, unsmoothed; bin size, 40 ms. (**F** to **K**) Six additional place cells from the hippocampus of different bats. Same notation as in (A). When a neuron had more than one place field, different fields were marked with different colors (K). The neuron in (J) was recorded in the cubic enclosure; the other neurons are from the rectangular-cuboid room.

dimension (Fig. 3J) and along each of the three major axes (Fig. 3, K and L), indicating that the entire available environment was represented rather uniformly by the population of place cells.

Most hippocampal neurons in rodents exhibit strong theta modulation of their firing rate, which can be readily observed in spike-train temporal autocorrelograms (*22*–*25*). However, it has been difficult to find firing-rate oscillations in the hippocampus of several other mammals, including wheeling monkeys (*26*) and crawling bats [(*3*, *5*); fig. S18]. But could theta rhythmicity occur during flight? We hypothesized this might be the case, because flight entails several conditions favorable for the generation and detection of theta rhythmicity, such as high-velocity movements (fig. S4), high firing rates (Fig. 2 and fig. S19), and strong oscillatory behaviors by the animal (fig. S20). Surprisingly, however, we found the opposite. The theta rhythmicity of hippocampal place cells was assessed by computing

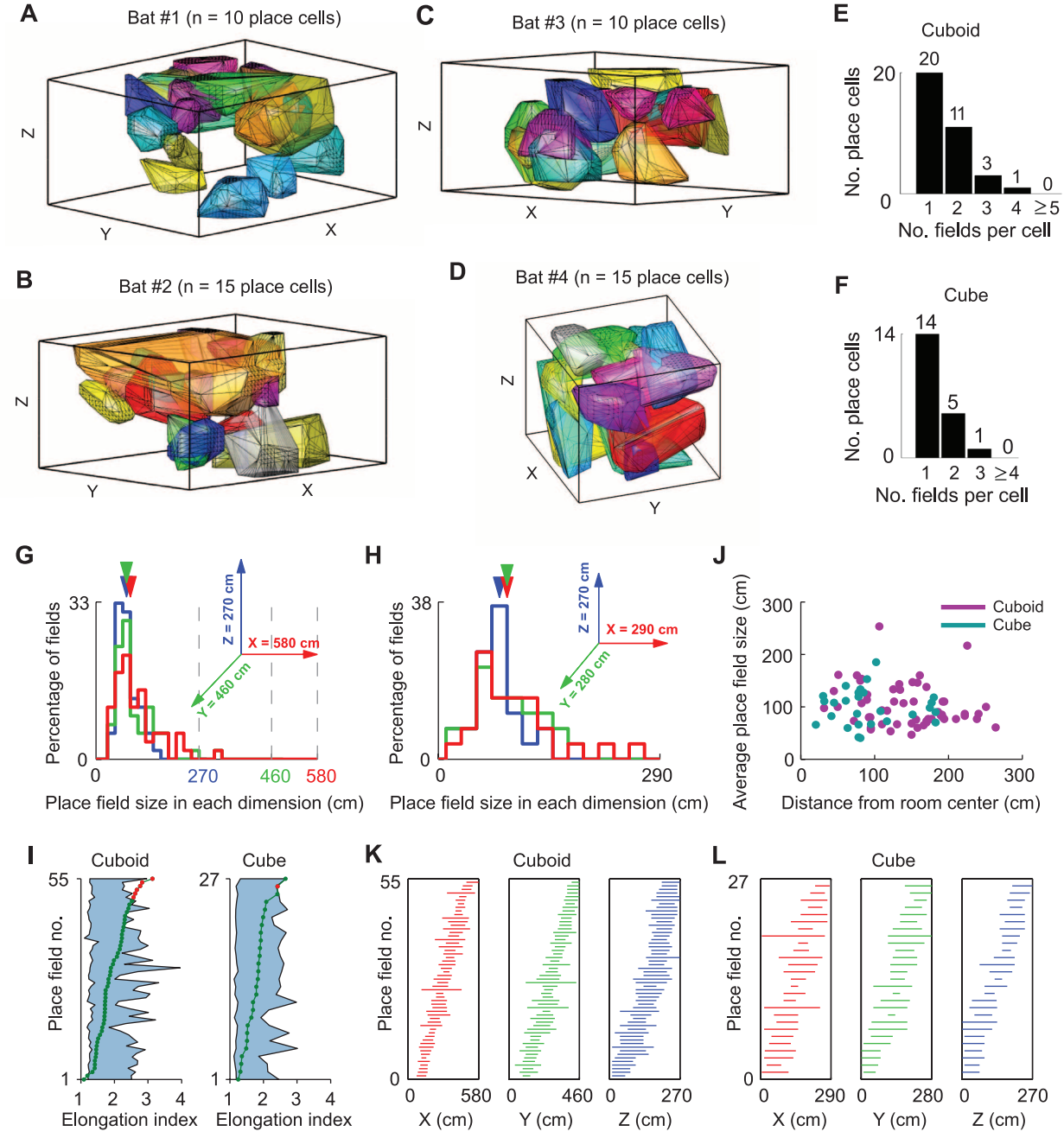


**Fig. 3. 3D space is encoded uniformly and nearly isotropically in the hippocampus of flying bats.** (**A** to **D**) All the place fields recorded from the hippocampus of four individual bats (different colors denote different neurons). Bats 1 to 3 (A) to (C) were tested in the cuboid-shaped flight-room, bat 4 (D) in the cubic enclosure. (**E** and **F**) Distribution of the number of place fields per neuron, in each experimental setup. (**G** and **H**) Distribution of place-field size in each dimension (different colors), in the rectangular-cuboid (G) and cubic setup (H). Color-matched arrowheads indicate median values. (**I**) Elongation indices for all place fields in both setups, sorted in ascending order. Shaded area, 95% confidence intervals (*19*). Only a small fraction of place fields had a shape significantly different from a sphere (9%, or 7/82 fields, red dots), whereas 91% of place fields were not statistically different from a sphere (green dots). (**J**) Average place-field size versus distance from room center in both setups (different colors); each symbol represents a single place field. (**K** and **L**) Locations and sizes of all place fields in each dimension of the room (*x*,*y*,*z*) in the cuboid (K) and cubic (L) setup; each horizontal line represents the extent of a single place field, sorted by position separately for *x*,*y*,*z*; same colors as in (G) and (H).

a standard "theta index" (Fig. 4, A to C, and fig. S21) (*19*), which has been used in previous studies in rats and bats to assess theta rhythmicity (*5*, *23*, *24*). A statistical shuffling procedure was applied for each individual neuron to test for significance (or lack thereof) of theta modulation in bat hippocampal neurons (*19*). Only 3.6% of the 3D place cells in both experimental setups (2/55 neurons) exhibited significant theta-modulated firing (*19*), but this rhythmicity was very weak (fig. S21) and, at the population level, was not different than would be expected by chance (binomial test, $P = 0.77$) (*19*). The degree of theta modulation of bat hippocampal neurons was stably low when comparing crawling versus the two flight setups (Fig. 4D), despite dramatic increases in movement velocity (speeding up almost two orders of magnitude: Fig. 4, D and E, and figs. S4 and S19) and a much higher firing rate of neurons during rapid flight (Fig. 4E and fig. S19). Theta rhythmicity was not correlated with the bat's echolocation rate (fig. S21H). Thus, we found a near-absence of spike-train theta rhythmicity in the bat hippocampus, both during crawling and during free flight. These results are strikingly different from the robust theta-rhythmic spiking of place cells in rodents (*1*) but are consistent with our previous reports in crawling bats (*3*, *5*). The near absence of theta modulation in the firing of hippocampal place cells in bats (this study) and monkeys (*26*) is incongruent with dual-oscillatory models of spatial coding (*1*, *2*).

What factors may shape the nearly isotropic 3D coding that we found in >90% of bat hippocampal place cells during flight? Bats are mammals that naturally move and navigate in 3D volumetric environments, and additionally their echolocation system provides them with volumetric 3D sensory information, including depth (*10*, *27*). Thus, isotropic 3D spatial coding might have evolved in bats because of the pressures to encode and retrieve 3D sensory information. This interpretation also implies possibly different encoding of 3D space in land-dwelling mammals that typically do not move volumetrically in 3D during ontogeny but instead rely mainly on horizontal self-motion cues. Indeed, a recent study (*16*) reported anisotropic coding in rat hippocampal neurons, with strong elongation of place fields in the vertical dimension [but see isotropic coding reported in a different study in rats (*9*) and discussion in (*10*, *28*)]. However, movement through 3D volumetric spaces is characteristic for many nonflying mammals, and we hypothesize that, as in bats, this could have created an evolutionary pressure to represent 3D volumetric position in the brain circuits of many species. The extent to which this prediction applies to humans is an intriguing question, because on one hand we evolved from monkeys that jumped across 3D volumes, but on the other hand we typically locomote along 2D surfaces. This will have to be studied in humans and monkeys in real and virtual 3D settings.

Finally, would these findings extend also to real-life navigation in the wild (*29*)? The average size of 3D place fields found here (~1 m) was consistent with the predictions of a computation model of 3D place cells, for room-sized environments (*30*); the same model also predicts place fields on the order of kilometers

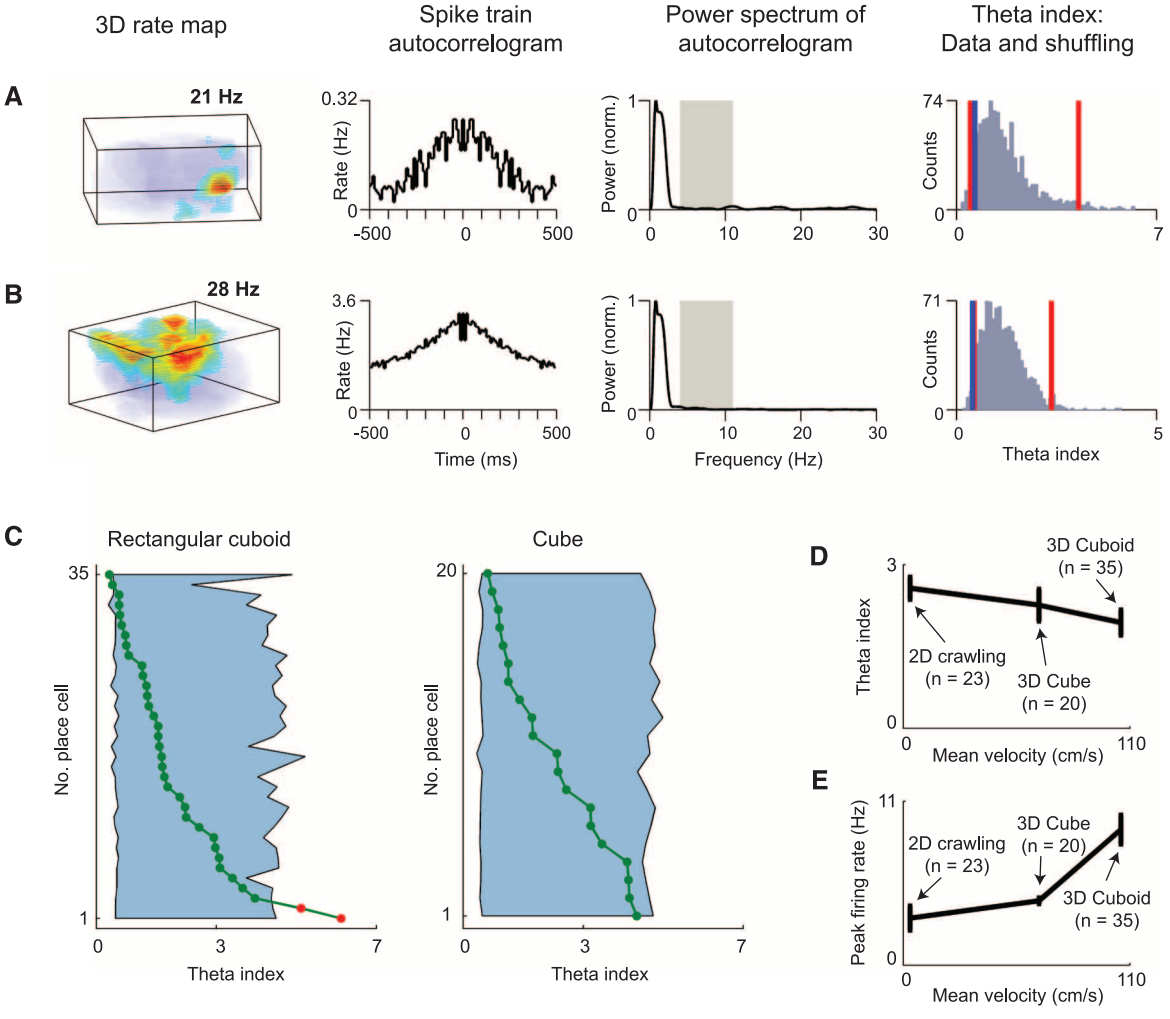


**Fig. 4. Near-absence of theta rhythmicity in the firing of bat hippocampal place cells during flight.** (**A** and **B**) Two example cells. From left to right: 3D color-coded rate maps, with peak firing rate indicated; spike-train temporal autocorrelograms; power spectrum of autocorrelogram; and shuffled distribution of theta indexes (red lines, 95% confidence intervals; blue line, actual theta index of the neuron) (*19*). There was a near-absence of power in the theta band (5 to 11 Hz, gray rectangle in the third column; power normalized to 1). See fig. S21 for additional examples. (**C**) Theta indexes for all place cells from the rectangular-cuboid flight room (left) and cubic flight enclosure (right). Neurons are sorted by theta-index values. Shaded area, 95% confidence intervals. Only a small fraction of place cells were significantly theta-modulated (red dots: 3.6%, or 2/55 of neurons in both setups together), whereas nearly all the place cells were not modulated (green dots: 96.4%, or 53/55 of neurons). (**D** and **E**) Theta indexes (D) and peak firing rates (E) as a function of the bat's velocity, under three different conditions (crawling, flying inside the cubic enclosure, or flying in the cuboid flight room).

in bats flying in their natural habitat. Further, navigation requires more than the hippocampal spatial signal: It also entails decision-making, goal-directed behaviors, sensory-motor integration, and other cognitive processes (mediated by brain structures such as the striatum, cerebellum, and prefrontal and parietal cortices). Thus, to elucidate the neural basis of real-life navigation in bats (*27*, *29*), it would be essential to record neural activity from the hippocampal formation (and additional brain structures) in bats navigating over distances of kilometers.

### References and Notes


1. P. Andersen, R. G. Morris, D. Amaral, T. Bliss, J. O'Keefe, *The Hippocampus Book* (Oxford Univ. Press, New York, 2007).
2. E. I. Moser, E. Kropff, M.-B. Moser, *Annu. Rev. Neurosci.* **31**, 69 (2008).
3. N. Ulanovsky, C. F. Moss, *Nat. Neurosci.* **10**, 224 (2007).
4. N. Ulanovsky, C. F. Moss, *Hippocampus* **21**, 150 (2011).
5. M. M. Yartsev, M. P. Witter, N. Ulanovsky, *Nature* **479**, 103 (2011).
6. T. Ono, K. Nakamura, H. Nishijo, S. Eifuku, *J. Neurophysiol.* **70**, 1516 (1993).
7. C. G. Kentros, N. T. Agnihotri, S. Streater, R. D. Hawkins, E. R. Kandel, *Neuron* **42**, 283 (2004).
8. A. D. Ekstrom *et al.*, *Nature* **425**, 184 (2003).
9. J. J. Knierim, B. L. McNaughton, G. R. Poe, *Nat. Neurosci.* **3**, 209 (2000).
10. N. Ulanovsky, *Curr. Biol.* **21**, R886 (2011).
11. C. D. Harvey, F. Collman, D. A. Dombeck, D. W. Tank, *Nature* **461**, 941 (2009).
12. E. J. Henriksen *et al.*, *Neuron* **68**, 127 (2010).
13. N. Ludvig, H. M. Tang, B. C. Gohil, J. M. Botero, *Brain Res.* **1014**, 97 (2004).
14. M. A. Wilson, B. L. McNaughton, *Science* **261**, 1055 (1993).
15. S. P. Jadhav, C. Kemere, P. W. German, L. M. Frank, *Science* **336**, 1454 (2012).
16. R. Hayman, M. A. Verriotis, A. Jovalekic, A. A. Fenton, K. J. Jeffery, *Nat. Neurosci.* **14**, 1182 (2011).
17. J. J. Knierim, B. L. McNaughton, *J. Neurophysiol.* **85**, 105 (2001).
18. K. J. Jeffery, R. L. Anand, M. I. Anderson, *Exp. Brain Res.* **169**, 218 (2006).
19. Materials and methods are avaliable as supplementary materials on *Science* Online.
20. This telemetry system did not allow recording of low-frequency local field potentials because of inherent high-pass limitations (*19*). The bat's wings hitting on the telemetry transmitter caused some recording artifacts (Fig. 1G and fig. S11), but these artifacts constituted only a small fraction of the flight time (3.6 ± 0.91% of the total flight time per day, mean ± SD). This fraction decayed to 0.11% after 9 recording days (fig. S11D), enabling us to collect neural spiking data with almost no movement-related interference.
21. A. A. Fenton *et al.*, *J. Neurosci.* **28**, 11250 (2008).
22. S. Royer, A. Sirota, J. Patel, G. Buzsáki, *J. Neurosci.* **30**, 1777 (2010).
23. R. F. Langston *et al.*, *Science* **328**, 1576 (2010).
24. T. J. Wills, F. Cacucci, N. Burgess, J. O'Keefe, *Science* **328**, 1573 (2010).
25. J. Koenig, A. N. Linder, J. K. Leutgeb, S. Leutgeb, *Science* **332**, 592 (2011).
26. E. Hori, E. Tabuchi, N. Matsumura, T. Ono, H. Nishijo, *Front. Behav. Neurosci.* **5**, 36 (2011).
27. N. Ulanovsky, C. F. Moss, *Proc. Natl. Acad. Sci. U.S.A.* **105**, 8491 (2008).
28. J. S. Taube, M. Shinder, *Hippocampus* **23**, 14 (2013).
29. A. Tsoar *et al.*, *Proc. Natl. Acad. Sci. U.S.A.* **108**, E718 (2011).
30. W. M. Brown, A. Bäcker, *Neural Comput.* **18**, 1511 (2006).


**Acknowledgments:** We thank A. Treves, D. Derdikman, J.-M. Fellous, L. Las, Y. Yovel, M. Ahrens, and C. Brody for comments on the manuscript; R. Raz, K. Kamenitz, and M. Geva-Sagiv for the 3D trajectory reconstruction system; C. Stengel for the neural telemetry system; B. Pasmantirer and G. Ankaoua for mechanical designs; A. Rubin and A. Averkin for assistance with neural recordings and video calibrations; S. Kaufman, T. Dayan, and S. Dror for bat training; M. Weinberg and A. Tuval for veterinary oversight; C. Ra'anan and R. Eilam for histology; and M. P. Witter for advice on reconstruction of tetrode-track locations. This study was supported by research grants from the European Research Council (ERC–NEUROBAT), the Human Frontiers Science Program (HFSP RGP0062/2009-C), the Israel Science Foundation (ISF 1017/08), and the Minerva Foundation to N.U. and a Lev-Zion predoctoral excellence fellowship to M.M.Y.

### Supplementary Materials

www.sciencemag.org/cgi/content/full/340/6130/367/DC1
Materials and Methods
Figs. S1 to S22
References

18 January 2013; accepted 21 February 2013
10.1126/science.1235338

# Developmental Decline in Neuronal Regeneration by the Progressive Change of Two Intrinsic Timers

**Yan Zou,[1]* Hui Chiu,[1]* Anna Zinovyeva,[2] Victor Ambros,[2] Chiou-Fen Chuang,[1]† Chieh Chang[1,3]†**

**Like mammalian neurons, *Caenorhabditis elegans* neurons lose axon regeneration ability as they age, but it is not known why. Here, we report that *let-7* contributes to a developmental decline in anterior ventral microtubule (AVM) axon regeneration. In older AVM axons, *let-7* inhibits regeneration by down-regulating LIN-41, an important AVM axon regeneration–promoting factor. Whereas *let-7* inhibits *lin-41* expression in older neurons through the *lin-41* 3′ untranslated region, *lin-41* inhibits *let-7* expression in younger neurons through Argonaute ALG-1. This reciprocal inhibition ensures that axon regeneration is inhibited only in older neurons. These findings show that a *let-7*–*lin-41* regulatory circuit, which was previously shown to control timing of events in mitotic stem cell lineages, is reutilized in postmitotic neurons to control postdifferentiation events.**

We use *Caenorhabditis elegans* to study developmental decline in neuronal regeneration (Fig. 1A) (*1*). As in vertebrates, advancing development leads to decreased axon regenerative capacity in *C. elegans* (Fig. 1C) (*2*–*4*). The timing mechanism that controls developmental decline in neuronal regeneration is poorly understood (*2*–*5*). Because heterochronic genes are implicated in regulating developmental timing and aging in *C. elegans* (*6*), we hypothesized that they might regulate developmental decline in neuronal regeneration. The heterochronic pathway involves a number of microRNA-regulated posttranscriptional genetic circuits (*7*, *8*), including an important interaction between the *let-7* microRNA and its direct target, *lin-41*, which encodes a tripartite motif (TRIM) protein (*9*, *10*). We show here that *let-7* and *lin-41* function in postmitotic neurons to time their differentiation and postdifferentiation events. Our study reveals that the intrinsic timing mechanism that controls developmental decline in neuronal regeneration depends on the progressive increase of *let-7* and the progressive decrease of *lin-41* in neurons, with *let-7*–*lin-41* reciprocal inhibition having a role in this process.

MicroRNA expression is either spatially restricted or temporally regulated in neuronal development (*11*–*14*). To explore the role of microRNAs in neuronal regeneration, we examined anterior ventral microtubule (AVM) axon regeneration in mutants defective in microRNA biogenesis, *dcr-1* and *alg-1 (15).* Although *dcr-1* hypomorphic mutant animals displayed normal AVM axon regeneration (fig. S1A), regenerating AVM neurons of adult *alg-1* mutants extended axons 2.5 times the length of those in adult wild-type animals (Fig. 1, B to D). In addition, regenerating axons of *alg-1* adults often displayed compact growth cones (fig. S1C). These regeneration phenotypes in adult *alg-1* mutants are reminiscent of those in wild-type animals at an earlier developmental stage (Fig. 1, B to D, and fig. S1), which suggests that *alg-1* mutations may retard a normal developmental decline in axon regeneration. Consistent with this conclusion, we observe that, although AVM axon regeneration in *alg-1* mutants is similar to that of wild-type animals at the larval L2

[1]Division of Developmental Biology, Cincinnati Children's Hospital Research Foundation, Cincinnati, OH 45229, USA. [2]RNA Therapeutics Institute and Program in Molecular Medicine, University of Massachusetts Medical School, Worcester, MA 01605, USA. [3]Department of Neurology and Neurosurgery, McGill University, Montreal, Quebec H3A 1B1, Canada.

*These authors contributed equally to this work.
†Corresponding author. E-mail: chieh.chang@cchmc.org (C.C.); chiou-fen.chuang@cchmc.org (C.-F.C.)